Applied Catalysis B: Environmental 239 (2018) 125–132

Contents lists available at ScienceDirect

Applied Catalysis B: Environmental

journal homepage: www.elsevier.com/locate/apcatb

# A hydrothermal approach to access active and durable sulfonated silica-ceramic carbon electrodes for PEM fuel cell applications

Reza Alipour Moghadam Esfahani, Reza B. Moghaddam, Iraklii I. Ebralidze, E. Bradley Easton*

*Electrochemical Materials Lab, Faculty of Science, University of Ontario Institute of Technology, 2000 Simcoe Street N, Oshawa, ON, Canada*

ARTICLE INFO

*Keywords:*
PEM fuel cell
Hydrothermal synthesis
Ceramic carbon electrode (CCE)
Oxygen reduction reaction (ORR)
Durability

ABSTRACT

We report on a one-step hydrothermal approach to synthesize Sulfonated Silica-Ceramic Carbon Electrode (HT-SS-CCE), a Nafion-free catalyst layer (CL) structure for proton exchange membrane fuel cells (PEMFC). This new approach to HT-SS-CCE synthesis gave rise to a more uniform distribution of the silicate within the CL and stabilizing the Pt nanoparticles (NPs) which further enhanced the activity and durability of electrode. In the initial assessment of the catalyst under three electrode cell experiments, the HT-SS-CCE showed enhanced activity towards the oxygen reduction reaction (ORR) compared with Nafion-based Pt/C. Furthermore, the HT-SS-CCE preserved a greater portion of its initial performance after the accelerated stress testing (AST) compared with Nafion-based Pt/C. This translated into higher performance and durability for HT-SS-CCE in fuel cell testing.

## 1. Introduction

On account of their green operation and high energy output, proton exchange membrane fuel cells (PEMFCs) have attracted a major consideration as a clean energy technology. Performance and stability are important concerns for PEMFC applications, thus tremendous attention has been paid to durability studies. In particular, the oxygen reduction reaction (ORR) is known to be the performance and durability bottleneck reaction in the cathodes of PEMFC [1–7]. Conventional cathode catalyst layers (CLs) consist of Pt/C blended with Nafion ionomer that serves as a proton conductor and binder. However, there are serious concerns that neither the carbon support nor the Nafion would withstand long-term operation under fuel cells conditions, causing (electro)/chemical and mechanical degradation. Such unwanted degradation will give rise to dramatic loss of performance [8–11]. As a key requirement for the effective implementation of fuel cells, their constructing materials should sustain long run operations [7,12,13].

A common approach to enhancing the stability of the carbon support is to blend it with a metals oxide, such as, $TiO_x$, $SnO_x$, $NbO_x$, $MoO_x$ and $SiO_2$ [14–22]. These have all been shown to increase stability through strong interaction with Pt nanoparticles (NPs), while also giving similar or better ORR activity and fuel cell performance [23,24]. However, these metals oxide also have a detrimental effect on the electrical conductivity of the support.

Silicate-based materials have been investigated in fuel cell CL as a proton conducting ionomer to replace Nafion in the CL. These electrode structures are referred to as ceramic carbon electrodes (CCE) [25–27]. In CCEs, the monomeric silanes are blended with Pt/C at room temperature and subsequently polymerized, forming a composite CL structure. Our group has demonstrated that sulfonated silica-ceramic carbon electrodes (SS-CCE) prepared by a room temperature sol-gel process have a high active surface area of Pt and highly promising fuel cell performance [28,29]. The silicate structure grows around the catalyst particles, which imports robustness to the catalyst structure. Such robustness may work to prevent known problems with long operation of Pt catalysts (e.g. dissolution and agglomeration). Also, their hygroscopic nature is the central reason for the SS-CCE to efficiently operate over a wider range of humidity condition than conventional Nafion-based CLs [30]. The hygroscopic character of SS-CCE is uniquely helpful in retaining and management of water within the CL, preventing the membrane from drying in low humidity and absorbing excess of water under high humidity conditions to prevent flooding of the CL. Recently, we have demonstrated that SS-CCEs also show enhanced durability in an operating PEMFC [28], though enhanced ORR activity has yet to be proven.

This paper presents a novel hydrothermal route to synthesize SS-CCE in an autoclave (i.e. HT-SS-CCE) as support material to Pt catalysts. The hydrothermal approach was used in an attempt to prepare a more evenly distributed silicate network throughout the CL compared to the room temperature sol-gel process. It was expected that the high

* Corresponding author.
*E-mail address:* brad.easton@uoit.ca (E.B. Easton).

https://doi.org/10.1016/j.apcatb.2018.07.077
Received 24 May 2018; Received in revised form 27 July 2018; Accepted 29 July 2018
Available online 30 July 2018
0926-3373/ 

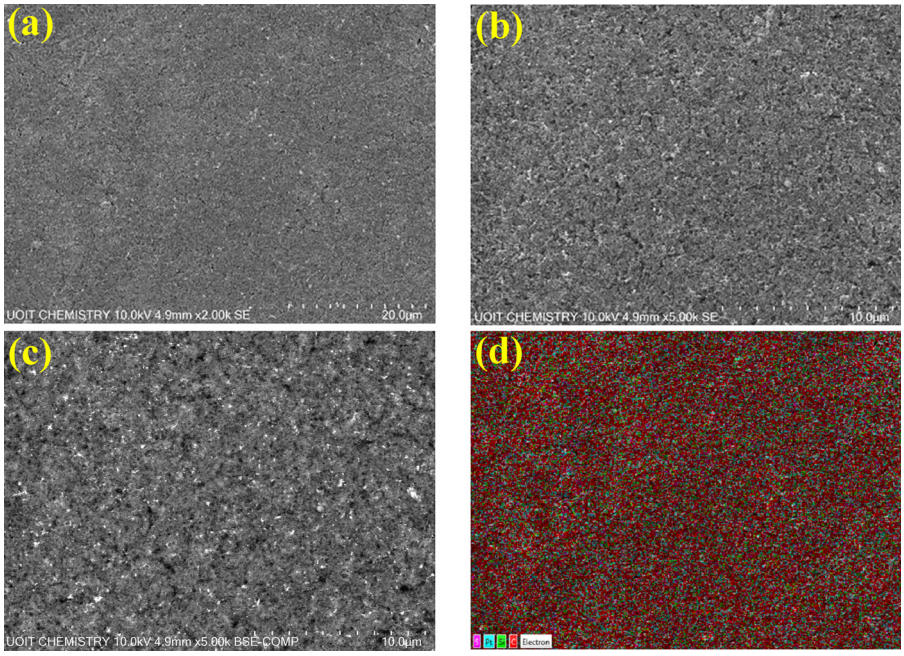


**Fig. 1.** (a) SEM images of HT-SS-CCE CL. (b), and (c) SEM images of HT-SS-CCE CL through secondary electrons and back-scattered electrons (d) EDX elemental mapping of HT-SS-CCE CL overlaid onto the SEM image in (a).

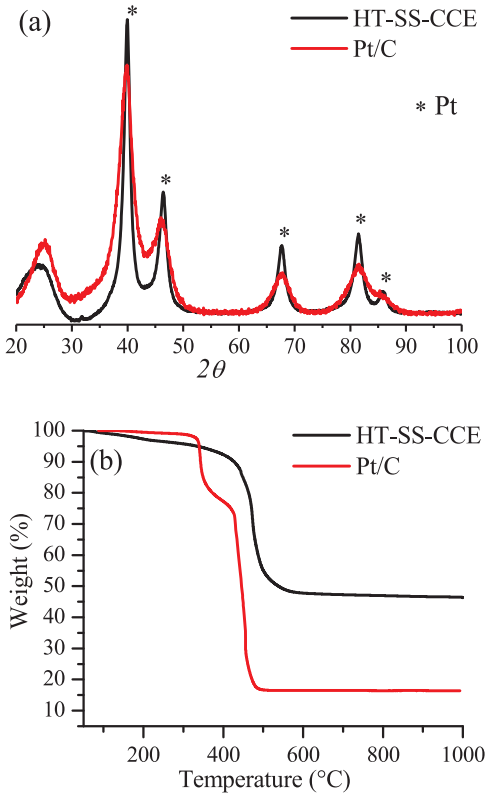


**Fig. 2.** (a) XRD patterns obtained for HT-SS-CCE and Nafion-based Pt/C CL. (b) TGA obtained from HT-SS-CCE and Nafion-based Pt/C CL.

temperature and pressure can provide more effective access of the monomers to a larger portion of the micropores in the carbon, which may further result in a more uniform and denser network of silane within the CL. Such uniform, dense silane network should offer more uniform water management, owing to the hygroscopic nature of the SS-CCE. It will be discussed that the multifunctional HT-SS-CCE acts not only as a binder, but it also enhances the durability and electroactivity. The HT-SS-CCE produced a sustained ORR activity under conventional three electrode setup, in accordance with its great longevity under fuel cell conditions.

## 2. Experimental

### 2.1. Chemicals

Commercial platinum catalyst 20 wt.% on carbon black Johnson Matthey, HiSPEC 3000 (Alfa Aesar). Gas diffusion layer (GDL) Elat LT1400 W single sided (NuVant Systems Inc.). 2-propanol ($C_3H_8O$) 99.5 wt.%, Methanol ($CH_4O$) 99.8 wt.%, Nafion® perfluorinated resin solution 5 wt.%, Ammonium hydroxide ($NH_4OH$) 28.0% $NH_3$ basis, tetraethylorthosilicate (TEOS), 3-(trihydroxysilyl)-1-propanesulfonic acid (TPS, 30–35% in water), sulfuric acid ($H_2SO_4$) 95–98 wt.%, were purchased from Sigma Aldrich. Nafion® membrane was purchased from Ion Power, Hydrogen, Nitrogen and oxygen gases were supplied in cylinders by PRAXAIR with 99.999% purity. All aqueous solutions were prepared using ultrapure water obtained from a Millipore Milli-Q system with resistivity > 18 MΩ cm.

### 2.2. Synthesis of electrodes

The HT-SS-CCE was prepared in an autoclave reactor. 20% Pt on carbon black (HiSPEC 3000) was mixed with deionized water and sonicated for 10 min, after which methanol and 6 M ammonium hydroxide were added to the solution. The catalyst mixture was mechanically stirred for 1 h, after which, TEOS and TPS were added drop-wise to achieve a 5:95 TPS/TEOS mole ratio at a constant total silane concentration of ca. 30%. This mixture was stirred for 2 h, and then the mixture was transferred to the autoclave reactor and treated at 110 °C for 70 h. The obtained HT-SS-CCE was spray deposited onto the GDL and the obtained electrodes were heat-treated at 130 °C for 30 min, then kept at 60 °C for 3 h. The HT-SS-CCE had Pt loading of 0.25 mg $cm^{-2}$, TEOS loading of 0.55 mg $cm^{-2}$ and TPS loading of 0.03 mg $cm^{-2}$. Also, Nafion-based electrodes were prepared with the same amount of Pt loading and Nafion loading of 0.65 mg $cm^{-2}$ (37.5 wt.%).

Membrane-electrode assemblies (MEAs) were fabricated by hot-pressing (150 kg $cm^{-2}$ for 90 s at 110 °C) the two identical electrodes

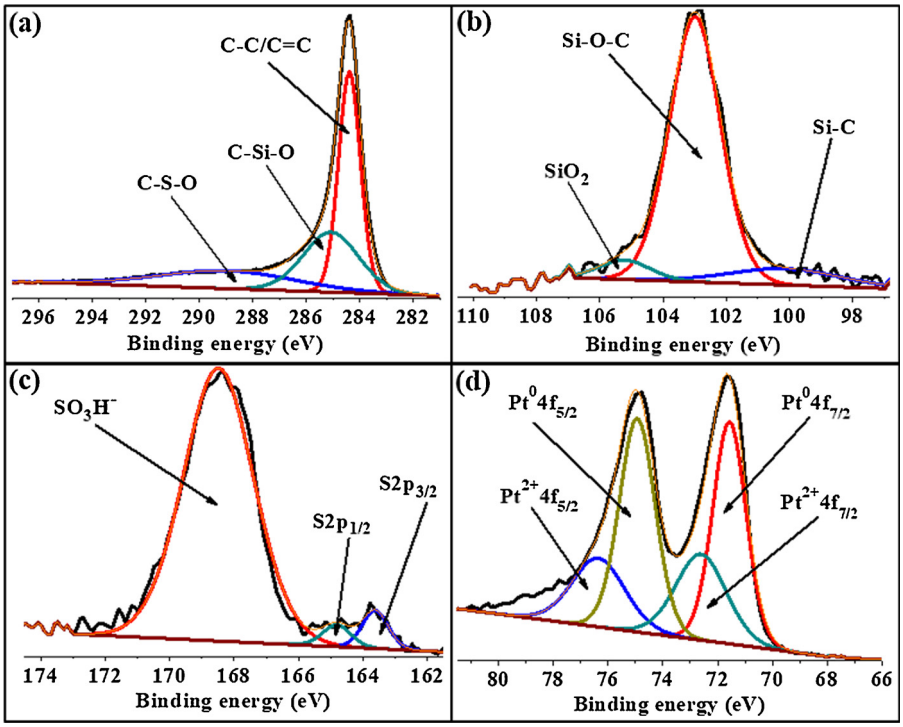


**Fig. 3.** XPS spectra of HT-SS-CCE, (a) C, (b) Si, (c) S and (d) Pt.

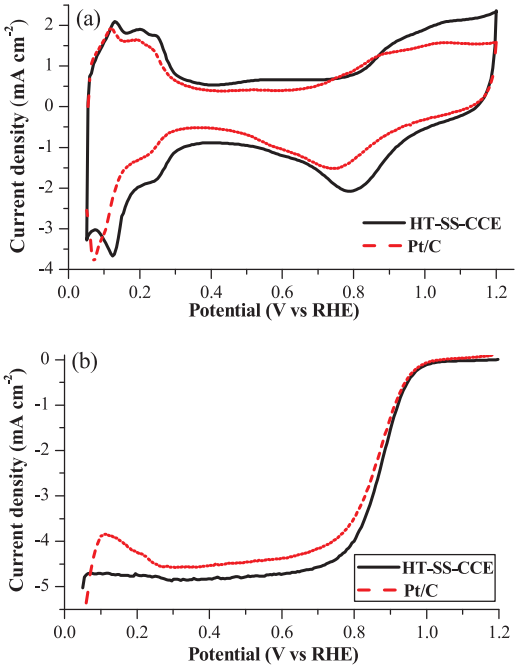


**Fig. 4.** (a) Comparisons of the CVs obtained for HT-SS-CCE and Nafion-based Pt/C recorded in $N_2$-purged 0.5 M $H_2SO_4$, scan rate of 10 mV $s^{-1}$. (b) Comparison of the ORR activity of HT-SS-CCE and Nafion-based Pt/C recorded in $O_2$-saturated 0.5 M $H_2SO_4$, scan rate of 5 mV $s^{-1}$, 1200 rpm.

across a Nafion® 212 membrane (Ion Power Inc.) using a Carver laboratory press equipped with a temperature-controlled heating block. MEAs were tested in a 5 $cm^2$ test fuel cell on a commercial fuel cell test station (Fuel Cell Technologies) controlled using Labview software.

### 2.3. Physical characterization

The phases and lattice parameters of the HT-SS-CCE and Pt/C were characterized by using X-ray diffraction (XRD) employing a Rigaku Ultima IV X-ray diffractometer system detector. The instrument employs Cu Kα radiation, (λ = 0.15418 nm) operating at 40 kV and 44 mA. Thermogravimetric analysis (TGA) was performed using a TA Instruments Q600 SDT thermal analyzer. Samples were heated from room temperature to 1000 °C at a rate of 10 °C $min^{-1}$ under flowing air (20 mL $min^{-1}$). The surface composition of the HT-SS-CCE catalyst was studied by X-ray photoelectron spectroscopy (XPS), employing Thermo Scientific K-Alpha Angle- Resolved system equipped with a monochromatic Al Kα (1486.7 eV) X-ray source and 180° double focusing hemispherical analyzer with 128 channel detector with effective charge compensation. Scanning Electron Microscopy (SEM) images were obtained using a Hitachi FlexSEM 1000 system equipped with an energy dispersive X-ray analyzer.

### 2.4. Electrochemical characterization of electrocatalysts

Electrochemical experiments were performed using either a Pine WaveDriver 20 potentiostat or a Solartron 1470 multichannel potentiostat coupled to a Solartron 1260 frequency response analyzer, controlled using Multistat software (Scribner Associates). The electrochemical evaluation of HT-SS-CCE was performed by immobilizing the sample onto the surface of a glassy carbon rotating disk electrode (Pine Instruments). 7 µL of obtained HT-SS-CCE was deposited onto the surface of the glassy carbon electrode (0.196 $cm^2$) and placed in oven to dry at 130°C for 15 min. This coated electrode served as the working electrode (Pt loading of 0.04 mg $cm^{-2}$) and was placed in a solution of 0.5 M $H_2SO_4$ along with a $Hg/HgSO_4$ reference electrode and Pt wire counter electrode. The potential of the of $Hg/HgSO_4$ reference electrode was calibrated regularly against the reversible hydrogen electrode (RHE) potential, which was determined to be +0.68 V vs RHE. All potential reported here have been corrected to the RHE scale.

Cyclic voltammetry (CV) and electrochemical impedance spectroscopy (EIS) experiments were performed in $N_2$-saturated solution. Impedance spectra were collected over a frequency range of 100 kHz–0.1 Hz at a DC bias potential of 0.425 $V_{RHE,}$ and an AC amplitude of 10 mV. ORR activity was assessed using linear sweep

**Table 1**
Electrochemical characterization of electrocatalysts.

| | 3 electrode cell | | | | Fuel cell | | | |
|---|---|---|---|---|---|---|---|---|
| Catalyst | Pt loading [mg $cm^{-2}$] | ECSA [$m^2 g^{-1}$] | I @0.9 [mA $cm^{-2}$] | Durability ECSA loss | Pt loading [mg $cm^{-2}$] | ECSA [$m^2 g^{-1}$] | Power density [mW $cm^{-2}$] | Durability ECSA loss |
| HT-SS-CCE | 0.04 | 82.47 | 1.54 | 45.7% | 0.25 | 85.25 | 915 | 49% |
| Nafion-Pt/C | 0.04 | 76.35 | 1.21 | 78.8% | 0.25 | 68.7 | 880 | 84% |

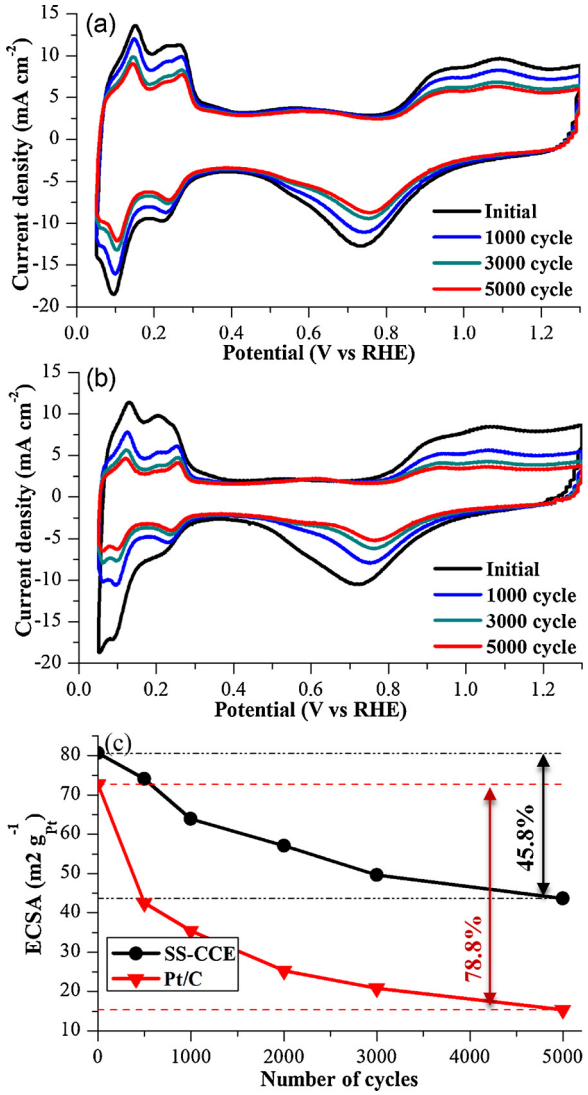


**Fig. 5.** Variation in the CV response of (a) HT-SS-CCE and (b) Nafion-based Pt/C during the AST. Measurements were made in $N_2$-purged 0.5 M $H_2SO_4$ at 25 °C at a sweep rate = 100 mV $s^{-1}$. (c) Variation in ECSA with number of potential cycles for each catalyst.

voltammetry at rotating disk electrode in $O_2$-saturated solution. electrocatalyst durability was assessed using an accelerated stress testing (AST) that involved repeated cycling of the working electrode potential between 0.05 and 1.3 $V_{RHE}$ at a scan rate of 100 mV $s^{-1}$, in an $N_2$-saturated 0.5 M $H_2SO_4$ solution. According to the United States Department of Energy testing protocols [31] this potential range assures the accelerated corrosion of the support as well as the sintering of Pt NPs. The electrode health was monitored by periodic CV and EIS assessment throughout the AST. In addition, ORR activity of electrocatalysts were assessed before and after the AST.

### 2.5. Fuel cell performance and durability

The fuel cell performance was measured at the beginning of life and after the AST for MEAs prepared from each electrode. The fuel cell tests were performed at 80 °C with feed gases of ($H_2$ and $O_2$) pressurized to 1 bar at the outlets of both anode and cathode side. Gases were humidified by passing through humidifier bottles prior to entering the cell. Electrode durability was examined by exposing each MEA to an AST. During the AST, the cathode was exposed to $N_2$ and the anode was exposed to $H_2$ with flow rates of 200 and 100 ml $min^{-1}$ respectively. The cell temperature was held constant at 25 °C, as was the anode and cathode humidifiers held constant at 25 °C. The AST consisted of 5000 potential cycles between 0.05 and 1.35 $V_{RHE}$, with periodic assessment of electrode health by CV and EIS. CV measurements were conducted to determine the electrochemically active surface area (ECSA). EIS measurements were used to confirm the mode of degradation during the durability test.

## 3. Results and discussion

### 3.1. Materials characterization

Fig. 1 shows SEM images obtained for the HT-SS-CCE spray coated on GDL, including an X-ray dispersive energy (EDS) elemental distribution map. The surface morphology of HT-SS-CCE appears smooth, owing to the evenly shaped fine particles on the surface (Fig. 1a). Fig. 1(b and c) shows the SEM images of HT-SS-CCE CL through secondary electrons and back-scattered electrons, which the EDS elemental mapping (Fig. 1d) further indicated the uniform distribution of the silicate within the catalyst structure. Fig. 2(a) shows the XRD profiles obtained for HT-SS-CCE. The XRD pattern displays signals associated with fcc Pt with an average crystallite size of ca. 3 nm. The narrower peaks are observed for the HT-SS-CCE compared with the Nafion-based CL, which can be attributed to the presence of silane that surrounds Pt NPs, a common feature that is also observed for metal oxide supported Pt catalysts [21,32]. Fig. 2(b) compares the TGA profiles for the HT-SS-CCE and Nafion-based CL. For the Nafion-based CL, the significant mass changes around 350–420 and 420–500 °C should be due to ionomer and carbon decompositions, respectively. While, for HT-SS-CCE degradation of carbon occurred at a higher temperature, 450–550 °C, due to the stabilizing effects of the silane. The analysis gave about 30 wt.% silicate that contained 5% TPS.

X-ray photoelectron spectroscopy was used to measure chemical states of C, Si, S, and Pt, where results are shown in Fig. 3. The XPS survey of C in the HT-SS-CCE deconvoluted into three constituting peaks. The most prominent peak at 284.3 eV is characteristic of the C—C bonding (Fig. 3a) [33,34]. The peak centered at 285.1 eV is attributed to the C—Si—O bond [35], suggestive of chemically attached sulfonated silane chain to the surface of carbon via a covalent C—Si bond and the peak located at 288.6 eV assigned to C—S—O bond [36]. The XPS spectral region for Si 2p appears to consist of three peaks associated to Si—C at 100.1 eV, Si—O—C at 102.8 eV and $SiO_2$ at 105.2 eV (Fig. 3b) [37,38]. Fig. 3c shows high-resolution of S 2p spectrum with doublet peaks at 163.6 eV and 164.8 eV assigned to S $2p_{3/2}$ and S $2p_{1/2}$ spectra for the S—C—S covalent bond and the peak at 168.4 attributed to the $SO_3H^-$ [39,40]. The Pt high-resolution spectrum shown in (Fig. 3d)

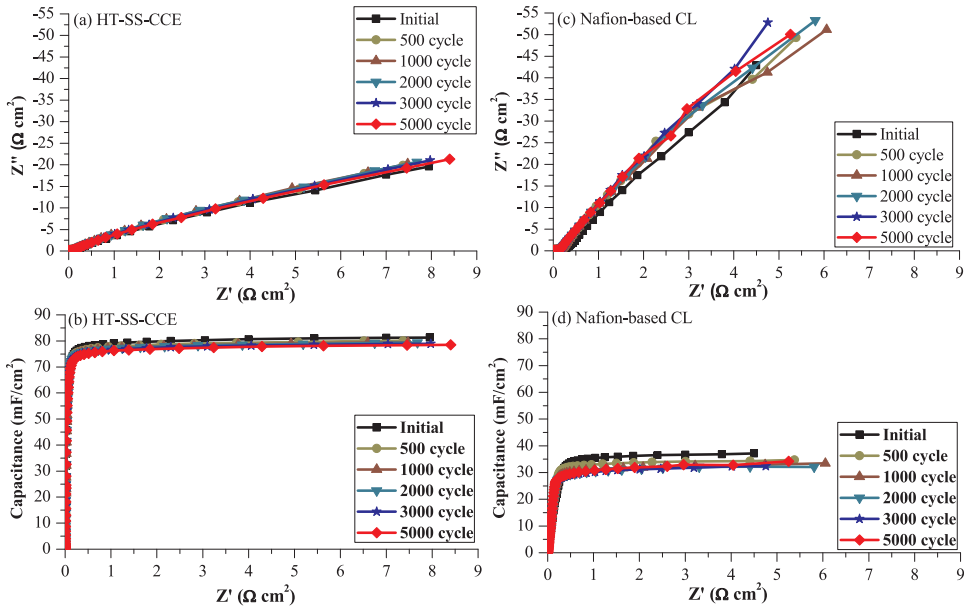


**Fig. 6.** Variation in the EIS response obtained by HT-SS-CCE during the AST, shown as (a) Nyquist and (b) capacitance plots. Variation in the EIS response obtained by Nafion-based Pt/C CL during the AST, shown as (c) Nyquist and (d) capacitance plots.

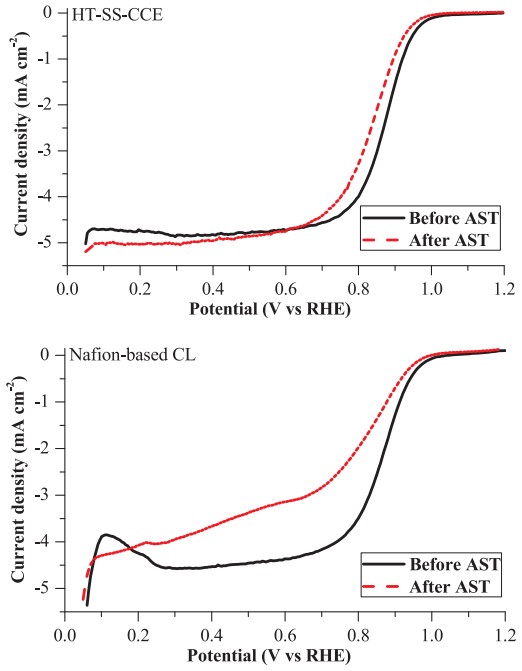


**Fig. 7.** Comparison of the ORR activity before (fresh) and after the AST for the (a) HT-SS-CCE and (b) Nafion-based Pt/C CL.

demonstrates spin-orbit splitting doublet peaks in the 4 f region attributed to the 4 $f_{7/2}$ and 4 $f_{5/2}$, where the deconvolution of the Pt spectrum reveals two pairs of doublet peaks at each region. The high intense doublet peaks at the binding energies of 71.6 eV and 74.9 eV are attributed to metallic Pt. The low-intensity doublet peaks at binding energies of 72.9 eV and 76.3 eV are assigned to $Pt^{2+}$ species due to surface oxide/hydroxide. The binding energy of Pt $4f_{7/2}$ reveals 0.6 eV positive shifts towards higher binding energy compared to the $4f_{7/2}$ conventional value of Pt/C. Such positive shifts, representative of extra positive charge on the Pt, may have been due to partial transfer of d electrons from Pt into the pi system of the electron accepting functional groups (e.g. sulfonates or silicates) in the HT-SS-CCE [41–44].

### 3.2. Electrochemical characterization of electrodes

Fig. 4a compares the CVs obtained for the HT-SS-CCE and the Nafion-based Pt/C CLs. Both electrocatalysts exhibit the typical electrochemistry of polycrystalline Pt, where hydrogen adsorption (cathodic) and desorption (anodic) dominate the voltammetry below 0.4 $V_{RHE}$. Oxide formation and stripping features are located at above 0.65 $V_{RHE}$. There is an earlier onset of the oxide formation for Pt/C than the HT-SS-CCE, which is consistent with its more negative potential for the completion of the oxide layer stripping on the cathodic sweep. The ECSA of each electrocatalyst was determined by integrating the peak area associated with under-potentially deposited hydrogen, $H_{UPD}$ (210 μC $cm_{Pt}^{-2}$). The HT-SS-CCE had a higher ECSA value compare with Nafion-based Pt/C, likely due to better distribution of the proton conductor within the CL. This further indicates that the CL made of the HT-SS-CCE contains more accessible active Pt sites.

Fig. 4b compares the ORR activity of HT-SS-CCE and Nafion-based Pt/C catalyst. The HT-SS-CCE shows a great ORR activity, with 1 $V_{RHE}$ onset potential of ORR (0.95 $V_{RHE}$ for Pt/C). The half-wave potential for the HT-SS-CCE was 0.87 $V_{RHE}$, some higher than 0.86 $V_{RHE}$ for Pt/C. As such, the HT-SS-CCE reached to an outstanding ORR activity, producing 1.54 mA $cm^{-2}$ at 0.9 $V_{RHE}$, greater than 1.21 mA $cm^{-2}$ for Nafion-based Pt/C.

The distinctive electroactivity of the HT-SS-CCE compared with Nafion-based Pt/C may be explained through strong metal-support interaction (SMSI) and/or synergetic effect that lead to significant changes in the d-band length of Pt and decrease the lattice parameter values, which should further weaken the too strong bonding between Pt and the adsorbed oxygenated species. Such adjustment is known to improve ORR activity of Pt catalyst [14,45–47]. Moreover, the HT-SS-CCE shows a higher limiting current, suggestive of higher porosity and permeability of the CL, further resulting in a lower kinetic barrier for ORR compared with Nafion-based Pt/C to accelerate kinetics of ORR at Pt [47–50]. A summary of key electrochemical parameters are presented in Table 1.

### 3.3. Durability of electrodes

Together with high electroactivity, durability is also a key characteristic of an electrocatalyst for fuel cell applications. One way to

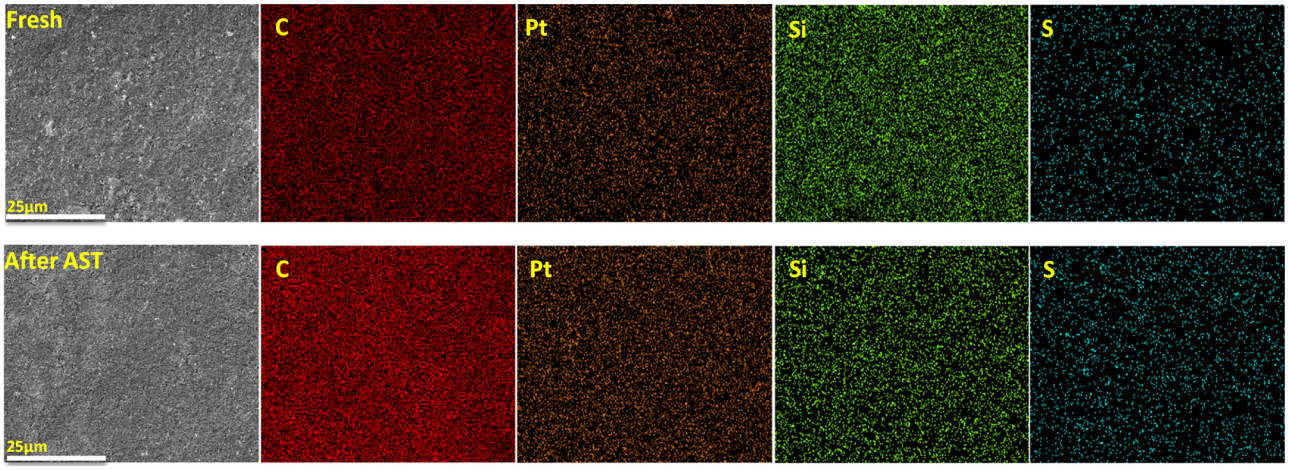


**Fig. 8.** Comparison of the SEM images and EDX elemental mapping obtained for the HT-SS-CCE before and after the AST.

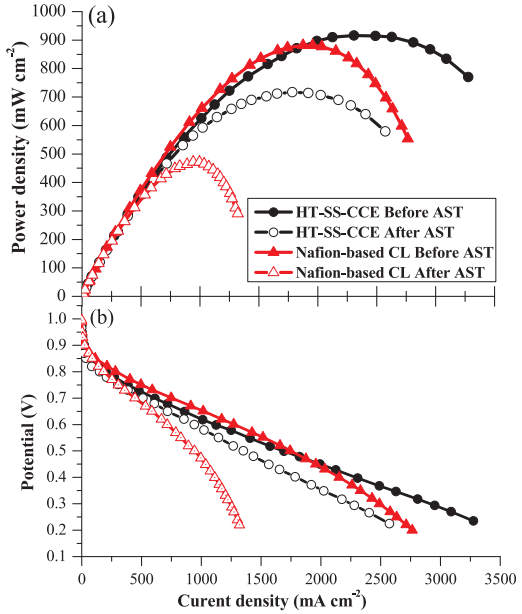


**Fig. 9.** Comparison of the fuel cell performance obtained using HT-SS-CCE and Nafion-based Pt/C electrode. Data is shown as (a) power density and (b) polarization curves. Measurements were made in a 5 $cm^2$ single cell PEMFC at 80 °C, using Pt loading of 0.25 mg $cm^{-2}$. $H_2$ flow rate of 100 N mL $min^{-1}$ 100% RH 1 bar BP; $O_2$ flow rate 200 N mL $min^{-1}$ 100% RH 1 bar BP, and Membrane = NRE 212.

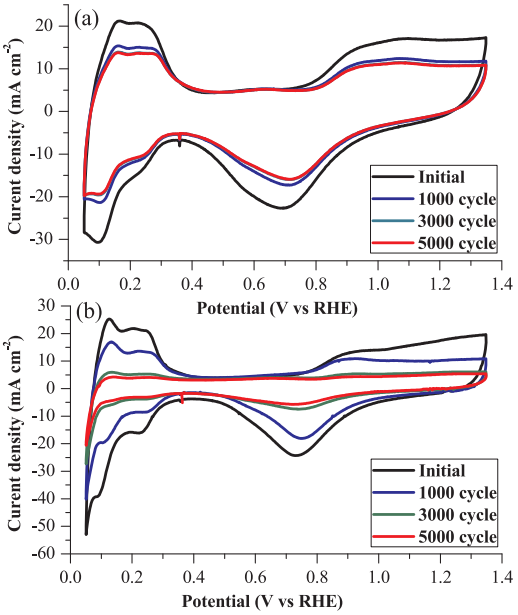


**Fig. 10.** Variation in the CV response of (a) HT-SS-CCE and (b) Nafion-based Pt/C during the AST. Measurements were made under fuel cell at 25 °C at a sweep rate of 100 mV $s^{-1}$.

evaluate durability is to monitor changes in ECSA during prolonged cycling, and whether it levels to decline itself in the ORR activity changes with cycling [51,52]. In this study the AST was conducted by subjecting the HT-SS-CCE and Nafion-based Pt/C catalysts to 5000 consecutive CV scans. Fig. 5 compares the change in CV response with cycling for both catalysts. As the test progressed, the HT-SS-CCE retained more of its original shape (Fig. 5a), while the Nafion-based Pt/C decayed more rapidly (Fig. 5b). After 5000 cycles, the ECSA of HT-SS-CCE decreased by 45.7%, compared with 78.8% decrease for the Nafion-based Pt/C. Such a large difference suggests that the organosilicate is effective in stabilizing the catalyst, which resulted in lesser extent of segregation or electro-dissolution of Pt NPs [53]. To have more numerical comparison of the voltammetric observations, Fig. 5c plots ECSA for both catalysts as a function of cycle number (i.e. obtained at selective points during potential scanning). To probe this further, EIS was also measured, as it can provide useful information about changes in conductivity and resistance in the CL under different conditions, as well as insight into degradation mechanisms [54,55]. Fig. 6 compares the EIS response for each electrode over the course of durability measurement, plotted as both Nyquist and series capacitance profiles. Both electrodes show good ionic conductivities, whereas the HT-SS-CCE displays a somewhat shorter Warburg length compared with the Nafion-based Pt/C. The Nyquist and capacitance plots obtained for HT-SS-CCE remained nearly unchanged throughout the AST. This indicates that excellent ionic and electronic conductivity were maintained throughout the test, and that there was no decay or corrosion of the support. For the Nafion-based Pt/C CL, a slight decrease in the Warburg length was observed over the AST, due to better wettability of the CL with progress of the test. The capacitance plots for Pt/C showed a decay over the course of the AST attributed to Pt dissolution/agglomeration [55–57].

To further examine the impact of the AST on the catalysts, voltammetric ORR was repeated for both electrocatalysts after completion of the AST (Fig. 7). As expected, there was only a small decrease in the ORR activity for the HT-SS-CCE, while a significant loss of activity can be observed for the Nafion-based Pt/C.

After the AST, SEM-EDX analysis was performed on the HT-SS-CCE

to study morphological and compositional changes with potential cycling (Fig. 8). The morphology of the HT-SS-CCE appears to have remained unchanged over the AST, where no significant change in the composition of the elements can also be found. These are consistent with the small changes in the ORR results and fuel cell polarization tests, demonstrating that the hydrothermal approach has led to a chemically robust catalyst, and that such robustness may have been a reason for the sustained electrochemical and fuel cell performances of the HT-SS-CCE.

### 3.4. Fuel cell performance

Fig. 9 compares the fuel cell performance of each electrode before and after the AST. Both HT-SS-CCE and Nafion-based Pt/C show similar performances initially, giving maximum power densities of 915 and 880 mW $cm^{-2}$, respectively. After the AST, a decrease in performance was observed for both electrodes. It is notable that the performance loss was more severe for the Nafion-based Pt/C compared with the HT-SS-CCE. The peak power density for the Nafion-based Pt/C decreased to 470 mW $cm^{-2}$ after the AST, corresponding to a 46.6% decline. Given the fact that the ECSA decayed by over 80% during the AST, a larger decline in fuel cell performance was rationally expected for the Nafion-based Pt/C. According to a previous study from this lab [28], there was considerable migration of Pt particles towards the membrane interface. The accumulation of Pt at this interface, where it is used most efficiently, may have partially mitigated the performance decline [58]. The peak power density obtained for the HT-SS-CCE decreased to 720 mW $cm^{-2}$ after the AST, which shows a remarkably better retention rate of performance compared with the Nafion-based Pt/C. This demonstrates that the enhanced electrochemical stability of HT-SS-CCE in a conventional cell correlates well with its better long-term performance under fuel cell conditions. It is also worth noting that the HT-SS-CCE composition reported here greatly outperforms SS-CCEs prepared by the room temperature sol-gel process used in our previous reports [29,30]. The hydrothermal process has brought the silane network into closer (and more effective) contact with the Pt NPs surfaces, creating a strong electronic interaction with Pt NPs. Such connection may slow down Ostwald ripening, agglomeration or migration into the bulk ionomer segment of the MEA, giving rise to enhanced performance and durability of the HT-SS-CCE. Consistently, Fig. 10, shows that voltammetric cycling (MEA, in fuel cell) of HT-SS-CCE (Fig. 10a) is much less prone to ESCA loss compared to conventional Nafion-based Pt/C (Fig. 10b), where ECSA value of HT-SS-CCE decreased by 49% while the Pt/C lost nearly 84% of its initial ECSA.

## 4. Conclusions

The HT-SS-CCE led to a catalyst layer with greater durability than the Nafion-based Pt/C. As such, compared with the traditional sol-gel process [28], the hydrothermal approach produced a more evenly distributed ionomer, which led to more effective bonding of the silane network to the carbon surface, and enhanced the ORR activity and fuel cell performance. The loss of ECSA for the HT-SS-CCE was nearly half of that for the Nafion-based Pt/C. Added to these observations, a slightly higher performance was obtained for HT-SS-CCE before the AST, which indicates it is not only more stable but also inherently more active than the Nafion-based Pt/C. To further amplify the significance of the HT-SS-CCE, the decline in peak power density was significantly less for that compared with the Nafion-based Pt/C. The HT-SS-CCE lost only 21.3% of its initial power, remarkably less than the 46.6% loss of power in the Nafion-based Pt/C.

## Acknowledgements

This work was supported by the Natural Sciences and Engineering Research Council (NSERC) of Canada through the Strategic Grants program (STPGP 479094-15), Ballard Power Systems, and University of Ontario Institute of Technology (UOIT). Support from the Canada Foundation for Innovation is also acknowledged. The authors thank Alan Young for useful discussion.

## References

[1] J. Choi, J.H. Jang, C.W. Roh, S. Yang, J. Kim, J. Lim, S.J. Yoo, H. Lee, Gram-scale synthesis of highly active and durable octahedral PtNi nanoparticle catalysts for proton exchange membrane fuel cell, Appl. Catal. B-Environ. 225 (2018) 530–537.
[2] J. Ying, J. Li, G.P. Jiang, Z.P. Cano, Z. Ma, C. Zhong, D. Su, Z.W. Chen, Metal-organic frameworks derived platinum-cobalt bimetallic nanoparticles in nitrogen-doped hollow porous carbon capsules as a highly active and durable catalyst for oxygen reduction reaction, Appl. Catal. B-Environ. 225 (2018) 496–503.
[3] S.M. Alia, C. Ngo, S. Shulda, M.-A. Ha, A.A. Dameron, J.N. Weker, K.C. Neyerlin, S.S. Kocha, S. Pylypenko, B.S. Pivovar, Exceptional oxygen reduction reaction activity and durability of platinum-nickel nanowires through synthesis and post-treatment optimization, ACS Omega 2 (2017) 1408–1418.
[4] H. Huang, K. Li, Z. Chen, L. Luo, Y. Gu, D. Zhang, C. Ma, R. Si, J. Yang, Z. Peng, J. Zeng, Achieving remarkable activity and durability toward oxygen reduction reaction based on ultrathin Rh-Doped Pt nanowires, J. Am. Chem. Soc. 139 (2017) 8152–8159.
[5] B.J. Hsieh, M.C. Tsai, C.J. Pan, W.N. Su, J. Rick, J.F. Lee, Y.W. Yang, B.J. Hwang, Platinum loaded on dual-doped TiO2 as an active and durable oxygen reduction reaction catalyst, NPG Asia Mater. 9 (2017) e403.
[6] Y. Gao, M. Hou, Z. Shao, C. Zhang, X. Qin, B. Yi, Highly effective oxygen reduction activity and durability of antimony-doped tin oxide modified PtPd/C electrocatalysts, RSC Adv. 5 (2015) 69479–69486.
[7] M.E. Scofield, H. Liu, S.S. Wong, A concise guide to sustainable PEMFCs: recent advances in improving both oxygen reduction catalysts and proton exchange membranes, Chem. Soc. Rev. 44 (2015) 5836–5860.
[8] J. Wu, X.Z. Yuan, J.J. Martin, H. Wang, J. Zhang, J. Shen, S. Wu, W. Merida, A review of PEM fuel cell durability: degradation mechanisms and mitigation strategies, J. Power Sources 184 (2008) 104–119.
[9] D.P. Wilkinson, J. St-Pierre, W. Vielstich, H.A. Gasteiger, A. Lamm (Eds.), Handbook of Fuel Cells: Fundamentals, Technology and Applications, vol. 3, John Wiley & Sons Ltd, 2003, pp. 611–626.
[10] H.A. Gasteiger, S.S. Kocha, B. Sompalli, F.T. Wagner, Activity benchmarks and requirements for Pt Pt-alloy, and non-Pt oxygen reduction catalysts for PEMFCs, Appl. Catal. B Environ. 56 (2005) 9–35.
[11] M.D. Gimenez-Lopez, A. Kurtoglu, D.A. Walsh, A.N. Khlobystov, Extremely stable platinum-amorphous carbon electrocatalyst within hollow graphitized carbon nanofibers for the oxygen reduction reaction, Adv. Mater. 2 (2016) 9103–9108.
[12] L. Dubau, L. Castanheira, F. Maillard, M. Chatenet, O. Lottin, G. Maranzana, J. Dillet, A. Lamibrac, J.C. Perrin, E. Moukheiber, A. ElKaddouri, G.D. Moor, C. Bas, L. Flandin, N. Caqué, A review of PEM fuel cell durability: materials degradation, local heterogeneities of aging and possible mitigation strategies, Wiley Interdiscip. Rev. Energy Environ. 3 (2014) 540–560.
[13] S. Sui, X. Wang, X. Zhou, Y. Su, S. Riffat, C.J. Liu, A comprehensive review of Pt electrocatalysts for the oxygen reduction reaction: nanostructure, activity, mechanism and carbon support in PEM fuel cells, J. Mater. Chem. A 5 (2017) 1808–1825.
[14] R. Alipour Moghadam Esfahani, A.H.A. Monteverde Videla, S. Vankova, S. Specchia, Stable and methanol tolerant Pt/TiOx-C electrocatalysts for the oxygen reduction reaction, Int. J. Hydrogen Energy 40 (2015) 14529–14539.
[15] R. Alipour Moghadam Esfahani, S. Vankova, A.H.A. Monteverde Videla, S. Specchia, Innovative carbon-free low content Pt catalyst supported on Mo-doped titanium suboxide (Ti3O5-Mo) for stable and durable oxygen reduction reaction, Appl. Catal. B Environ. 201 (2017) 419–429.
[16] N.R. Elezovica, V.R. Radmilovic, N.V. Krstajic, Platinum nanocatalysts at metal oxide based supports for low temperature fuel cells applications, RSC Adv. 6 (2016) 6788–6801.
[17] C. Odetola, L.N. Trevani, E.B. Easton, Photo enhanced methanol electrooxidation: further insights into Pt and TiO2 nanoparticle contributions, Appl. Catal. B Environ. 210 (2017) 263–275.
[18] Z. Zhang, J. Liu, J. Gu, L. Su, L. Cheng, An overview on metal oxide materials as electrocatalysts and supports for polymer electrolyte fuel cells, Energy Environ. Sci. 7 (2014) 2535–2558.
[19] K. Sasaki, L. Zhang, R.R. Adzic, Niobium oxide-supported platinum ultra-low amount electrocatalysts for oxygen reduction, Phys. Chem. Chem. Phys. 10 (2008) 159–167.
[20] Y.N. Wu, S.J. Liao, J.H. Zeng, Investigating the addition of silicon oxide to carbon: effects of amount and heat treatment on anti-aggregation and electrochemical performance of Pt catalysts, J. Power Sources 196 (2011) 1112–1117.
[21] Y. Zhang, J. Zang, L. Dong, X. Cheng, Y. Zhao, Y. Wang, A Ti-coated nano-SiC supported platinum electrocatalyst for improved activity and durability in direct methanol fuel cell, J. Mater. Chem. A Mater. Energy Sustain. 2 (2014) 10146–10153.
[22] H. Schmies, A. Bergmann, J. Drnec, G. Wang, D. Teschner, S. Kühl, D.J.S. Sandbeck, S. Cherevko, M. Gocyla, M. Shviro, M. Heggen, V. Ramani, R.E. Dunin-Borkowski, K.J.J. Mayrhofer, P. Strasser, Unravelling degradation pathways of oxide-supported Pt fuel cell nanocatalysts under in situ operating conditions, Adv. Energy Mater. 8 (2018) 1701663.
[23] S.Y. Huang, P. Ganesan, B.N. Popov, Electrocatalytic activity and stability of titania-

supported platinum palladium electrocatalysts for polymer electrolyte membrane fuel cell, J. Am. Chem. Soc. 2 (2012) 825–831.
[24] R. Alipour Moghadam Esfahani, L. Miguel Rivera Gavidia, G. García, E. Pastor, S. Specchia, Highly active platinum supported on Mo-doped titanium nanotubes suboxide (Pt/TNTS-Mo) electrocatalyst for oxygen reduction reaction in PEMFC, Renew. Energy 120 (2018) 209–219.
[25] B. Habibi, S. Ghaderi, Synthesis, characterization and electrocatalytic activity of Co@Pt nanoparticles supported on carbon-ceramic substrate for fuel cell applications, Int. J. Hydrogen Energy 40 (2015) 5115–5125.
[26] B. Habibi, N. Delnavaz, Carboneceramic supported bimetallic Pt-Ni nanoparticles as an electrocatalyst for oxidation of formic acid, Int. J. Hydrogen Energy 36 (2011) 9581–9590.
[27] B. Habibi, N. Delnavaz, Electrocatalytic oxidation of formic acid and formaldehyde on platinum nanoparticles decorated carbon-ceramic substrate, Int. J. Hydrogen Energy 35 (2010) 8831–8840.
[28] R. Alipour Moghadam Esfahani, H.M. Fruehwald, F. Afsahi, E. Bradley Easton, Enhancing fuel cell catalyst layer stability using a dual-function sulfonated silica-based ionomer, Appl. Catal. B Environ. 232 (2018) 314–321.
[29] J.I. Eastcott, K.M. Yarrow, A.W. Pedersen, E.B. Easton, Fuel cell electrode structure containing sulfonated organosilane-based proton conductor, J. Power Sources 197 (2012) 102–106.
[30] J.I. Eastcott, E.B. Easton, Sulfonated silica-based fuel cell electrode structure for low humidity application, J. Power Sources 245 (2014) 487–494.
[31] US DoE 2014 Annual Progress Report V. Fuel Cells, (2014) (Accessed December 2015). http://www.hydrogen.energy.gov/annual progress14fuelcells.html.
[32] R. Alipour Moghadam Esfahani, I.I. Ebralidze, S. Specchia, E.B. Easton, A fuel cell catalyst support based on doped titanium suboxides with enhanced conductivity, durability and fuel cell performance, J. Mater. Chem. A 6 (2018) 14805–14815.
[33] C. Wang, D. Sun, K. Zhuo, H. Zhang, J. Wang, Simple and green synthesis of nitrogen-, sulfur-, and phosphorus-co-doped carbon dots with tunable luminescence properties and sensing application, RCS. Adv. 4 (2014) 54060–54065.
[34] J.P. Paraknowitsch, Y. Zhang, B. Wienert, A. Thomas, Nitrogen- and phosphorus-co-doped carbons with tunable enhanced surface areas promoted by the doping additives, Chem. Commun. 49 (2013) 1208–1210.
[35] R. Bywalez, H. Karacuban, H. Nienhaus, C. Schulz, H. Wiggers, Stabilization of mid-sized silicon nanoparticles by functionalization with acrylic acid, Nanoscale Res. Lett. 7 (2012) 76.
[36] X. Zhang, Y. Huang, P. Liu, Enhanced electromagnetic wave absorption properties of poly(3,4-ethylenedioxythiophene) nanofiber-decorated graphene sheets by non-covalent interactions, Nano-Micro Lett. 8 (2016) 131–136.
[37] C.T. Lee, L.H. Tsai, Y.H. Lin, G.R. Lin, A chemical vapor deposited silicon rich silicon carbide P-N junction based thin-film photovoltaic solar cell, ECS J. Solid State Sci. Technol. 1 (2012) Q144–Q148.
[38] W.J. Choi, Y.J. Chung, Y.H. Kim, J. Han, Y.K. Lee, K. Kong, H. Chang, Y.K. Lee, B.G. Kim, J.O. Lee, Drawing circuits with carbon nanotubes: scratch-induced graphoepitaxial growth of carbon nanotubes on amorphous silicon oxide substrates, Sci. Rep. 4 (2014) 5289.
[39] C. Xu, Q. Han, Y. Zhao, L. Wang, Y. Li, L. Qu, Sulfur-doped graphitic carbon nitride decorated with graphene quantum dots for an efficient metal-free electrocatalyst, J. Mater. Chem. A 3 (2015) 1841–1846.
[40] L. Qie, W. Chen, X. Xiong, C. Hu, F. Zou, P. Hu, Y. Huang, Sulfur-Doped Carbon with Enlarged Interlayer Distance as a High-Performance Anode Material for Sodium-Ion Batteries, Adv. Sci. 2 (2015) 1500195.
[41] D.M. Han, Z.P. Guo, R. Zeng, C.J. Kim, Y.Z. Meng, H.K. Liu, Multiwalled carbon nanotube-supported Pt/Sn and Pt/Sn/$PMo_{12}$ electrocatalysts for methanol electrooxidation, Int. J. Hydrogen Energy 34 (2009) 2426–2434.
[42] Y. Zhang, J. Zang, L. Dong, X. Cheng, Y. Zhao, Y. Wang, A Ti-coated nano-SiC supported platinum electrocatalyst for improved activity and durability in direct methanol fuel cell, J. Mater. Chem. A Mater. Energy Sustain. 2 (2014) 10146–10153.
[43] G. Long, X. Li, K. Wan, Z. Liang, J. Piao, P. Tsiakaras, Pt/$C_{N\text{-}doped}$electrocatalysts: superior electrocatalytic activity for methanol oxidation reaction and mechanistic insight into interfacial enhancement, Appl. Catal. B Environ. 203 (2017) 541–548.
[44] B.A. Pereira, F. Laplante, M. Chaker, D. Guay, Functionally modified macroporous membrane prepared by using pulsed laser deposition, Adv. Funct. Mater. 17 (2007) 443–450.
[45] Z. Zhang, J. Liu, J. Gu, L. Su, L. Cheng, An overview on metal oxide materials as electrocatalysts and supports for polymer electrolyte fuel cells, Energy Environ. Sci. 7 (2014) 2535–2558.
[46] J. Greeley, I.E.L. Stephens, A.S. Bondarenko, T.P. Johansson, H.A. Hansen, T.F. Jaramillo, J. Rossmeisl, I. Chorkendorff, J.K. Nørskov, Alloys of platinum and early transition metals as oxygen reduction electrocatalysts, Nat. Chem. 1 (2009) 552–556.
[47] A. Pătru, A. Rabis, S.E. Temmel, R. Kotz, T.J. Schmidt, Pt/$IrO_2$–$TiO_2$ cathode catalyst for low temperature polymer electrolyte fuel cell-Application in MEAs, performance and stability issues, Catal. Today 262 (2016) 161–169.
[48] J. Zhang, M.B. Vukmirovic, Y. Xu, R. Mavrikakis, R.R. Adzic, Controlling the catalytic activity of platinum-monolayer electrocatalysts for oxygen reduction with different substrates, Angew. Chem. Int. Ed. 44 (2005) 2132–2135.
[49] X. Huang, Z. Zhao, L. Cao, Y. Chen, E. Zhu, Z. Lin, M. Li, A. Yan, A. Zettl, Y.M. Wang, X. Duan, T. Mueller, Y. Huang, High-performance transition metal-doped Pt3Ni octahedra for oxygen reduction reaction, Science 348 (2015) 1230–1234.
[50] S. Mukerjee, S. Srinivasan, M.P. Soriaga, J. McBreen, Role of structural and electronic properties of Pt and Pt Alloys on electrocatalysis of oxygen reduction, J. Electrochem. Soc. 142 (1995) 1409.
[51] R. Borup, J. Meyers, B. Pivovar, Y.S. Kim, R. Mukundan, N. Garland, D. Myers, M. Wilson, et al., Scientific aspects of polymer electrolyte fuel cell durability and degradation, Chem. Rev. 107 (2007) 3904–3951.
[52] J. Wu, X.Z. Yuan, J.J. Martin, H. Wang, J. Zhang, J. Shen, S. Wu, W. Merida, A review of PEM fuel cell durability: degradation mechanisms and mitigation strategies, J. Power Sources 184 (2008) 104–119.
[53] E.B. Easton, Z.G. Qi, A. Kaufman, P.G. Pickup, Chemical modification of proton exchange membrane fuel cell catalysts with A sulfonated silane, Electrochem. Solid-State Lett. 4 (2001) A59–A61.
[54] E.B. Easton, P.G. Pickup, An electrochemical impedance spectroscopy study of fuel cell electrodes, Electrochim. Acta 50 (2005) 2469–2474.
[55] F.S. Saleh, E.B. Easton, Diagnosing degradation within PEM fuel cell catalyst layers using electrochemical impedance spectroscopy, J. Electrochem. Soc. 159 (2012) B546–B553.
[56] F.S. Saleh, E.B. Easton, Assessment of the ethanol oxidation activity and durability of Pt catalysts with or without a carbon support using electrochemical impedance spectroscopy, J. Power Sources 246 (2014) 392–401.
[57] O. Reid, F.S. Saleh, E.B. Easton, Application of the transmission line EIS model to fuel cell catalyst layer durability, ECS Trans. 61 (2014) 25–32.
[58] R.L. Borup, J.R. Davey, F.H. Garzon, PEM fuel cell electrocatalyst durability measurments, J. Power Sources 163 (2006) 76–81.